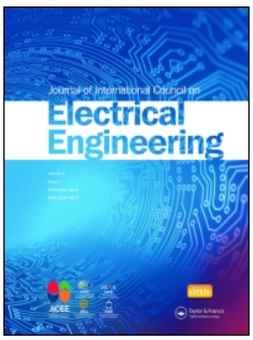

Taylor & Francis
Taylor & Francis Group

Journal of International Council on Electrical Engineering

ISSN: (Print) 2234-8972 (Online) Journal homepage: http://www.tandfonline.com/loi/tjee20

Development of partitioned stator flux-switching machines for electric vehicles

Christopher H. T. Lee, W. K. Lee & K. T. Chau

To cite this article: Christopher H. T. Lee, W. K. Lee & K. T. Chau (2017) Development of partitioned stator flux-switching machines for electric vehicles, Journal of International Council on Electrical Engineering, 7:1, 276-281, DOI: 10.1080/22348972.2017.1387330

To link to this article: https://doi.org/10.1080/22348972.2017.1387330

Published online: 03 Nov 2017.

JOURNAL OF INTERNATIONAL COUNCIL ON ELECTRICAL ENGINEERING, 2017
VOL. 7, NO. 1, 276–281
https://doi.org/10.1080/22348972.2017.1387330

Taylor & Francis
Taylor & Francis Group

Development of partitioned stator flux-switching machines for electric vehicles

Christopher H. T. Lee, W. K. Lee and K. T. Chau

Department of Electrical and Electronic Engineering, The University of Hong Kong, Hong Kong

ABSTRACT

In this paper, three advanced partitioned stator flux-switching permanent-magnet (PS-FSPM) machines with different number of phases, namely the 3-phase, the 4-phase, and the 5-phase are comprehensively compared. Owing to the higher-phase topology, better fault-tolerability and higher power density can be achieved. On the other hand, higher-phase machine suffers from the problem of relatively lower cost-effectiveness. Hence, trade-off between different criteria should be considered to fulfill various situations. In particular, all the PS-FSPM machines are highly favorable for the electric vehicle applications, while all of their key performances are analyzed with the support of the finite element method.

ARTICLE HISTORY
Received 21 September 2016
Accepted 29 September 2017

KEYWORDS
Partitioned stator; flux-switching; electric vehicle; multi-phase

1. Introduction

Because of the rising concerns on energy utilization and environmental protection, the development of the electric vehicles (EVs) has been accelerating [1–3]. As the major component of the EV technology, the electric machines have to offer several key distinctions, namely high efficiency, high power density, high controllability, wide-speed range, maintenance-free operation, and high fault-tolerability [4–6]. The permanent-magnet (PM) machines, which can accomplish most of the goals, have drawn many attentions in the past few decades [7–9]. Based on the flux-linkage patterns and the PM arrangements, the PM machines can be classified as three major types, namely the doubly-salient permanent-magnet (DSPM) machine, the flux-reversal permanent-magnet (FRPM) machine, and the flux-switching permanent-magnet (FSPM) machine [10–12]. Owing to the bipolar flux-linkage characteristic and flux concentration performance, the FSPM machine has been regarded as the most promising candidate for the EV applications [13–15].

Same as the other traditional machines, the FSPM machine normally adapts the outer-stator inner-rotor topology for most of the applications [16–18]. With this conventional topology, both the PM materials and armature windings are allocated within the outer stator, so that the inner space of the rotor part is wasted. To improve the situation, the partitioned stator (PS) FSPM machine, which purposely arranges an addition partition inside its inner space, is proposed [19,20]. Based on the PS-FSPM structure, the PM materials can be transferred from the outer stator to the inner partition, such that the winding slot areas in the outer stator can be enlarged. However, the existing PS-FSPM machine focuses mostly on the typical 3-phase topology, while the comparisons or discussions on the structure with higher-phase are still literally absent.

This paper aims to newly develop the PS-FSPM machines with higher-phase topology, purposely for the EV applications. With the higher-phase structure, better fault-tolerability and higher power density can be potentially achieved. In addition, the discussions on the cost-effectiveness are also included. The design criteria and principles of operation for the proposed higher-phase machines will be discussed. The machine performances will be analyzed based on the finite element methods (FEM) and then quantitatively compared with the commonly employed counterparts.

2. PS-FSPM machines

Figure 1 shows the three PS-FSPM machines with different topologies, namely the 3-phase 12/10-pole topology, the 4-phase 16/12-pole topology, and the 5-phase 20/14-pole topology. Due to the fact that all these PS-FSPM machines have the same principle of operation as compared with its predecessors, the design equations of the pole arrangement can be extended from that of the profound FSPM machine [14]. All the proposed PS-FSPM

CONTACT Christopher H. T. Lee htlee@eee.hku.hk

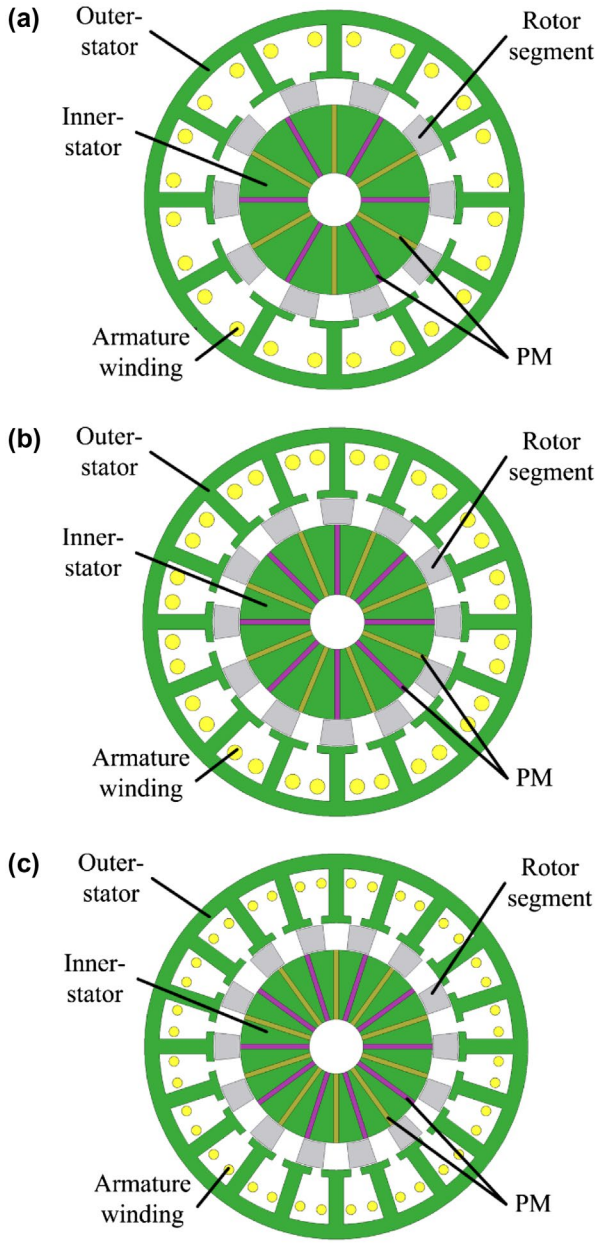

Figure 1. Proposed PS-FSPM machines: (a) 3-phase, (b) 4-phase, and (c) 5-phase.

machines employ the double-stator sandwiched-rotor structure, while the machine construction of the proposed machines is similar to those applied to the commonly developed machines [5].

The armature windings and the PM materials are installed in the outer-stator and the inner-stator of all three machines, respectively. To improve the control flexibility, the concentrated winding arrangement is employed for all the winding sets. Full-bridge converter circuits with different number of phases are implemented to the corresponding machines accordingly.

To illustrate the bipolar flux-linkage characteristics of the PS-FSPM machines, the flux flow patterns of the

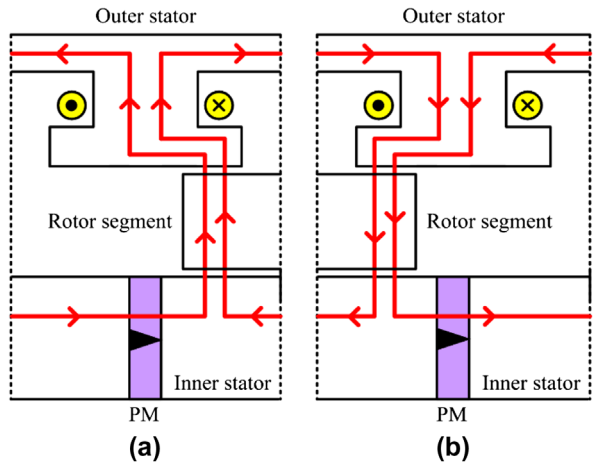

Figure 2. Flux flow patterns of PS-FSPM machines: (a) Position 1 and (b) Position 2.

PS-FSPM machine is shown in Figure 2. To be specific, when the sandwiched-rotor of the proposed machine rotates from position 1 to 2, the flux-linkages interchange its polarities accordingly. Therefore, the fundamental characteristics of the FSPM machines, i.e. the bipolar flux-linkage patterns, are provided. In this case, it can be expected the proposed PS-FSPM machines can offer higher power and torque densities than the unipolar counterparts do [13].

To offer the fair comparison environment, all the major machine dimensions, namely the outside diameters, the inside diameters, the stack lengths, the airgap lengths, and the slot-fill factors are set equal. Meanwhile, to prevent the magnetic saturations and the severe core losses, the values of the pole arcs, the pole heights, and the current densities are optimized.

3. Operation principles

All three proposed PS-FSPM machines can be operated with the bipolar conduction operation, which is similar to those applied to the profound FSPM machine [5]. To be specific, the armature current I_{arm} with the sinusoidal pattern is applied in accordance with the status of the bipolar flux-linkage Ψ, and hence the positive electromagnetic torque T can be generated. This operation scheme is sometimes known as the brushless AC (BLAC) conduction scheme, as shown in Figure 3. Upon the BLAC conduction scheme, the PS-FSPM machines can effectively comply the injected armature currents with its corresponding back electromotive force (EMF) waveforms, such that the torque ripple can be purposely minimized. The corresponding sinusoidal armature currents for the 3-phase PS-FSPM machine can be described as:

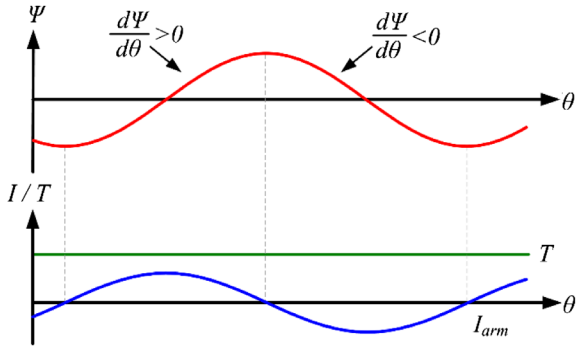

Figure 3. Theoretical operating waveforms.

$$\begin{cases} i_a = I_{\text{peak}} \sin\theta \\ i_b = I_{\text{peak}} \sin(\theta + (2\pi/3)) \\ i_c = I_{\text{peak}} \sin(\theta - (2\pi/3)) \end{cases} \quad (1)$$

where i_a, i_b, i_c and I_{peak} are the corresponding armature currents and the peak value of the phase currents, respectively. In the meantime, the corresponding conduction schemes for both 4-phase and 5-phase PS-FSPM machines are described in (2) and (3), respectively as:

$$\begin{cases} i_a = I_{\text{peak}} \sin\theta \\ i_b = I_{\text{peak}} \sin(\theta + (\pi/2)) \\ i_c = I_{\text{peak}} \sin(\theta + \pi) \\ i_d = I_{\text{peak}} \sin(\theta + (3\pi/4)) \end{cases} \quad (2)$$

$$\begin{cases} i_a = I_{\text{peak}} \sin\theta \\ i_b = I_{\text{peak}} \sin(\theta + (2\pi/5)) \\ i_c = I_{\text{peak}} \sin(\theta + (4\pi/5)) \\ i_d = I_{\text{peak}} \sin(\theta + (6\pi/5)) \\ i_e = I_{\text{peak}} \sin(\theta + (8\pi/5)) \end{cases} \quad (3)$$

where i_d, and i_e are the corresponding armature currents. As compared with the 3-phase machine, the higher-phase machines can potentially achieve higher power density based on the same current limitation of each phase. In contrast, the higher-phase machines suffer from relatively higher control complexity.

4. Machine performances analysis

All three PS-FSPM machines are compared based on the fair environments where the key design data are listed in Table 1. By the support of the FEM, all machine performances can be simulated and then quantitatively

Table 1. Key design data of PS-FSPM machines.

Items	3-phase	4-phase	5-phase
Outside diameter (mm)	156.0	156.0	156.0
Inside diameter (mm)	22.0	22.0	22.0
Airgap length (mm)	0.5	0.5	0.5
Stack length (mm)	120	120	120
Stator pole number	12	16	20
Rotor pole number	10	12	14
Number of phases	3	4	5
Slot-fill factor (%)	60	60	60
Number of turns	140	92	75

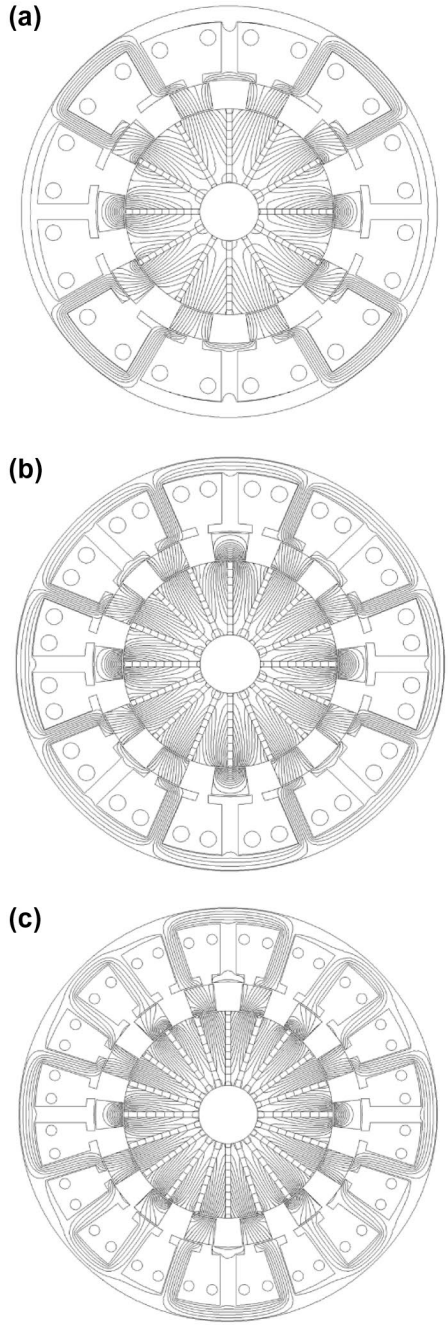

Figure 4. Magnetic field distributions of the proposed PS-FSPM machines: (a) 3-phase, (b) 4-phase, and (c) 5-phase.

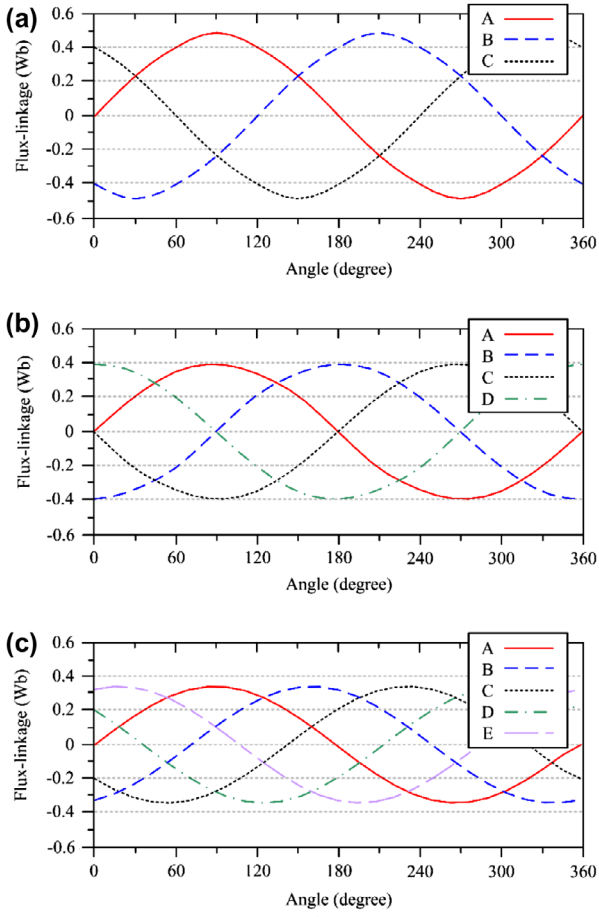

Figure 5. Flux-linkage waveforms of PS-FSPM machines: (a) 3-phase, (b) 4-phase, and (c) 5-phase.

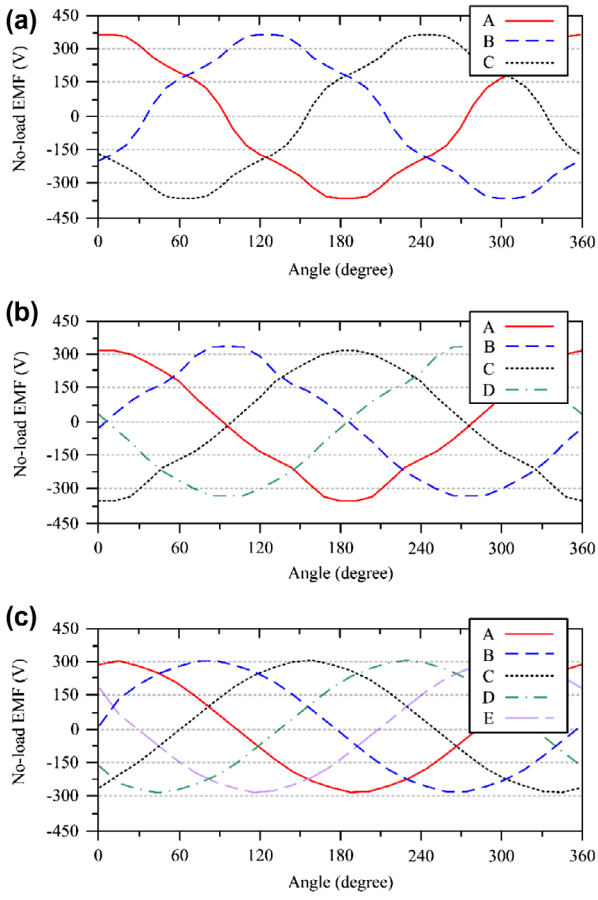

Figure 6. No-load EMF waveforms of PS-FSPM machines: (a) 3-phase, (b) 4-phase, and (c) 5-phase.

compared. In this paper, JMAG-Designer is adopted to perform the FEM analysis. The magnetic field distributions of all the proposed machines at no-load condition are shown in Figure 4. The results show that the flux distributions of all machines are well balanced where no severe saturation is observed.

Firstly, the flux-linkages of all machines are shown in Figure 5. It can be shown that all the flux-linkages consist of the bipolar waveforms with the balanced patterns. These flux-linkages illustrate the symmetrical pattern with almost no distortion so that the pole-pair arrangements of all these machines are confirmed to be correct. As compared with the higher-phase machines, the 3-phase machine consists of larger winding areas, so that larger number of armature windings can be installed. Hence, the 3-phase machine can achieve the largest flux-linkage amplitude among the group.

Secondly, the no-load EMF waveforms of these PS-FSPM machines at the base speed of 1000 rpm are shown in Figure 6. The results show that all PS-FSPM machines consist of the more sinusoidal-like patterns, such that it can be confirmed that the proposed machines are capable for the BLAC conduction scheme. As expected, because of the largest flux-linkage magnitude, the no-load EMFs generated by the 3-phase machine are relatively higher than those by its counterpart do. However, due to the fact that the higher-phase machines consist of larger number of conduction phases, it can be anticipated the higher-phases machines should be able to produce higher power and torque densities as compared with its counterparts do.

In the third place, the output torques of the proposed PS-FSPM machines are simulated and as shown in Figure 7. It can be shown that the average torques at rated conditions of the 3-phase machine, the 4-phase machine, and the 5-phase machine are 18.4 Nm, 20.8 Nm, and 22.1 Nm, respectively. As aforementioned, the 5-phase machine can achieve the highest torque value within the comparing group.

Apart from the average torque values, the torque ripples of the machines are also carefully analyzed. The torque ripple value T_{ripple} can be obtained based on the following relationship:

$$T_{\text{ripple}} = \frac{T_{\text{max}} - T_{\text{min}}}{T_{\text{avg}}} \times 100\% \tag{4}$$

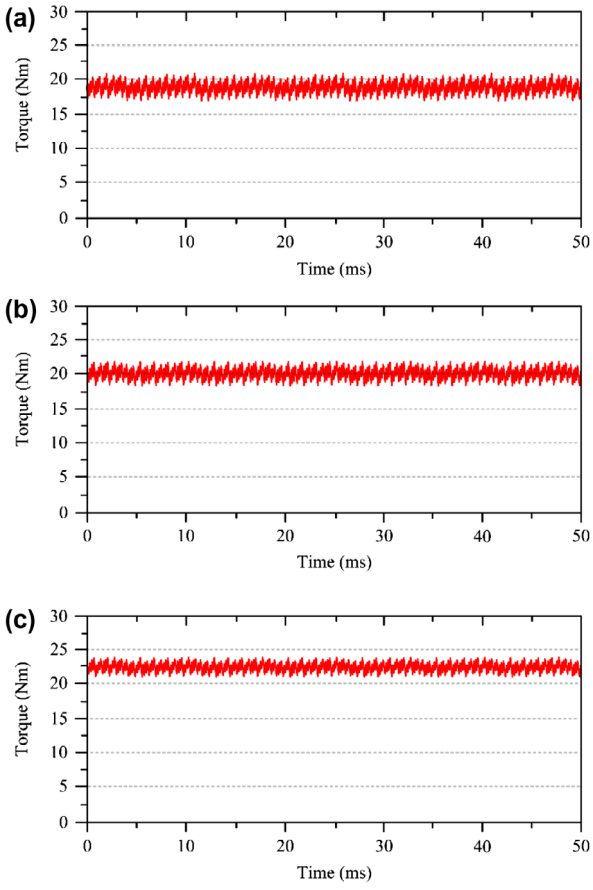

Figure 7. Steady torque waveforms of PS-FSPM machines: (a) 3-phase, (b) 4-phase, and (c) 5-phase.

Table 2. Key machine performance comparisons.

Items	3-phase	4-phase	5-phase
Rated power (W)	1900	2100	2300
Rated torque (Nm)	18.4	20.8	22.1
Rated torque ripple (%)	16.4	13.5	12.8
Material cost (US)	34.9	45.8	51.6
Power / cost (W/US)	54.4	45.9	44.6
Torque / cost (Nm/US)	0.53	0.45	0.43
Fault-tolerability	Low	Moderate	High

where T_{max}, T_{min}, and T_{avg} are the maximum torque value, the minimum torque value, and the average torque value, respectively. The obtained torque ripples of the 3-phase machine, the 4-phase machine, and the 5-phase machine are 16.4, 13.5 and 12.8%, respectively, which are all comparable to that produced from the profound FSPM machines [5].

Finally, the concept of the cost-effectiveness and the fault-tolerability are also included for the comprehensive comparisons. Relying on the raw materials of the current market prices, the material costs of the PS-FSPM machine are obtained. Due to the higher number of phases, the higher-phase machines have to bear the shortcomings of larger PM materials consumptions. Consequently, lower cost-effectiveness is resulted. On the other hand, with the higher possibility to offer healthy armature windings for remediation operation, the higher-phase machine instead can provide larger fault-tolerability than its counterparts do. For better presentation, the major comparisons of all three machines are listed in Table 2.

5. Conclusion

In this paper, three PS-FSPM machines with different topologies, namely the 3-phase topology, the 4-phase topology, and the 5-phase topology have been thoroughly studied and quantitatively compared. With the higher number of conduction phases, the 5-phase machine can definitely offer the best power and torque densities as compared with its lower-phase counterparts do. The 5-phase candidate can also provide higher fault-tolerability, yet it suffers from lower cost-effectiveness than its lower-phase counterparts do. On the other hand, the 3-phase PS-FSPM machine holds the opposite situation as compared with the 5-phase one. Hence, trade-off decisions should be made for different scenarios.

Disclosure statement

No potential conflict of interest was reported by the authors.

Funding

This work was supported by the Hong Kong Research Grants Council, Hong Kong Special Administrative Region, China [Project number 17200614].

Notes on contributors

Christopher H. T. Lee received the B.Eng. (first class honors) degree, and PhD degree both in electrical engineering from Department of Electrical and Electronic Engineering, The University of Hong Kong, Hong Kong. During the PhD study, he was co-supervised by Prof. K. T. Chau and Prof. C. C. Chan. He currently serves as the Honorary Assistant Professor in the alma mater. His research interests include electric machines and drives, renewable energies, and electric vehicle technologies. In these areas, he has published 2 book chapters, and about 30 technical papers. Dr Lee received the Croucher Foundation Fellowship 2016/2017 to support his postdoctoral research.

W. K. Lee received his BSc (Eng.) in electrical engineering and MSc (Eng) in industrial engineering from The University of Hong Kong. He also got MBA degree from The Chinese University of Hong Kong. After earning more than ten years of engineering experience in public service, he joined The University of

Hong Kong in 1988 for teaching and research, and currently serves as the Principal Lecturer. His main research interests include demand side performance, load signature, smartness reliability, and renewable energy systems. He has been one of the examiners of two professional examinations in Hong Kong for more than ten years. He also participates regularly as advisors, assessors and committee members for government and professional bodies.

K. T. Chau received his BSc (Eng.) degree with first class honors, MPhil degree, and PhD degree from The University of Hong Kong, Hong Kong, all in electrical and electronic engineering. He joined the alma mater in 1995, and currently serves as a Professor in the Department of Electrical and Electronic Engineering. His main research interests include electric vehicle technologies, renewable energy systems, and machines and drives. In these areas, he has published 7 books, 9 book chapters, and more than 250 refereed journal papers. Prof. Chau is a Fellow of the IEEE, the IET, and the HKIE. He has served as Chairs and Organizing Committee Member for many international conferences. He has received many awards, including the Chang Jiang Chair Professorship, the Environmental Excellence in Transportation Award for Education, Training and Public Awareness, and the Award for Innovative Excellence in Teaching, Learning and Technology.

ORCID

Christopher H. T. Lee http://orcid.org/0000-0001-5132-4126

References

[1] Ehsani M, Rahman KM, Toliyat HA. Propulsion system design of electric and hybrid vehicles. IEEE Trans Ind Electron. 1997 Feb;44(1):19–27.
[2] Chau KT, Chan CC. Emerging energy-efficient technologies for hybrid electric vehicles. Proc IEEE. 2007 Apr;95(4):821–835.
[3] Chau KT, Li WL, Lee CHT. Challenges and opportunities of electric machines for renewable energy (invited paper). Prog Electromagnet Res B. 2012;42:45–74.
[4] Zhu ZQ, Howe D. Electrical machines and drives for electric, hybrid, and fuel cell vehicles. Proc IEEE. 2007 Apr;95(4):746–765.
[5] Chau KT, Chan CC, Liu C. Overview of permanent-magnet brushless drives for electric and hybrid electric vehicles. IEEE Trans Ind Electron. 2008 Jun;55(6):2246–2257.
[6] Cheng M, Hua W, Zhang J, et al. Overview of stator-permanent magnet brushless machines. IEEE Trans Ind Electron. 2011 Nov;58(11):5087–5101.
[7] Cheng M, Chau KT, Chan CC, et al. Control and operation of a new 8/6 doubly salient permanent magnet motor drive. IEEE Trans Ind Appl. 2003 Sept;39(5):1363–1371.
[8] Li Y, Mi CC. Doubly salient permanent-magnet machine with skewed rotor and six-state commutating mode. IEEE Trans Magn. 2007 Sept;43(9):3623–3629.
[9] Chau KT. Electric vehicle machines and drives – design, analysis and application. Singapore: Wiley-IEEE Press; 2015.
[10] Wang C, Nasar SA, Boldea I. Three-phase flux reversal machine (FRM). IEE Proc-Electric Power Appl. 1999 Mar;146(2):139–146.
[11] Liu C, Chau KT, Jiang JZ. A permanent-magnet hybrid brushless integrated-starter-generator for hybrid electric vehicles. IEEE Trans Ind Electron. 2010 Dec;57(12):4055–4064.
[12] Cao R, Mi C, Cheng M. Quantitative comparison of flux-switching permanent-magnet motors with interior permanent magnet motor for EV, HEV, and PHEV applications. IEEE Trans Magn. 2012 Aug;48(8):2374–2384.
[13] Hoang E, Ben-Ahmed AH, Lucidarme J. Switching flux permanent magnet polyphased macines. In: Proc Eur Conf Power Electron Appl; Trondheim, Norway; 1997. p. 903–908.
[14] Chen JT, Zhu ZQ. Winding configurations and optimal stator and rotor pole combination of flux-switching PM brushless AC machines. IEEE Trans Energy Convers. 2010 Jun;25(2):293–302.
[15] Deodhar RP, Pride A, Iwasaki S, et al. Performance improvement in flux-switching PM machines using flux diverters. IEEE Trans Ind Appl. 2014;50(2):937–978.
[16] Pollock C, Pollock H, Barron R, et al. Flux-switching motors for automotive applications. IEEE Trans Ind Appl. 2006;42(5):1177–1184, Sept./Oct.
[17] Hua W, Cheng M, Zhu ZQ, et al. Analysis and optimization of back EMF waveform of a flux-switching permanent magnet motor. IEEE Trans Energy Convers. 2008 Aug;23(3):727–733.
[18] Zhu ZQ, Chen JT. Advanced flux-switching permanent magnet brushless machines. IEEE Trans Magn. 2010 Jun;46(6):1447–1453.
[19] Awah CC, Zhu ZQ, Wu ZZ, et al. Comparison of partitioned stator switched permanent magnet machines having single- or double-layer windings. IEEE Trans Magn. 2016 Jan;52(1):9500310.
[20] Zhu ZQ, Wu ZZ, Liu X. A partitioned stator variable flux reluctance machine. IEEE Trans Energy Convers. 2016 Mar;31(1):78–92.